10th Brazilian Congress on Manufacturing Engineering
August 05th-07th, 2019, São Carlos, SP, Brazil

THE INFLUENCE OF THERMAL VARIABLES OF SOLIDIFICATION ON MICROSTRUCTURE AND HARDNESS OF CU-8.5 WT% SN ALLOY

Givanildo Alves dos Santos
Ricardo Aparecido da Cruz
Maurício Silva Nascimento
Antonio Tadeu Rogério Franco
Carlos Frajuca
Francisco Yastami Nakamoto
Federal Institute of Education, Science and Technology of São Paulo, Zip Code 01109-010, São Paulo, Brazil
ricardoapcruz@ifsp.edu.br, givanildo@ifsp.edu.br, mauriciofisico@gmail.com, frajuca@gmail.com, nakamoto@ifsp.edu.br

Vinícius Torres dos Santos
Márcio Rodrigues da Silva
Educacional Center of Fundação Salvador Arena, Zip Code 09850-550, São Bernardo do Campo, Brazil
vinicius.ts1@hotmail.com; marcio.rdrgs.slv@gmail.com

Gilmar Ferreira Batalha
Polytechnic School of Engineering of the University of Sao Paulo, Zip Code 05508-900, São Paulo, SP, Brazil
gfbatalha@gmail.com

Antonio Augusto Couto
Institute of Nuclear and Energy Research, IPEN, Zip Code 05508-000, São Paulo, SP, Brazil
acouto@ipen.br

Manuel Venceslau Canté
São Paulo State Faculty of Technology of East Zone, FATEC-ZL, Zip Code 03694-000, São Paulo, Brazil
cantemvc@gmail.com

Abstract. *The Cu-8.5wt% Sn alloy is similar to the UNS C51200 phosphor bronze, a material commonly used in the manufacture of machine elements and electrical contacts. Concomitantly with the solidification of this bronze occurs the formation of a eutectoid mixture (detrimental to subsequent forming processes). We present here a study on the influence of the thermal variables of solidification on the microstructure and the hardness of that alloy. The unidirectional solidification technique was used for the acquisition of thermal data and metallographic analysis was performed with the use of optical microscopy to characterize the microstructure of the material as well as to measure the dendrite arm spacing. We performed hardness tests on samples from the columnar zone of the casting: six longitudinal samples and six transverse ones. The results showed that the hardness of the material tends to decrease as the dendrite arm spacing increases, as the tip growth rate decreases or as the cooling rate decreases. There is also a slight decrease in the amount of eutectoid mixture toward locations with higher tip cooling rate.*

Keywords: *Cu-8.5 wt% Sn alloy, Solidification, Microstructure, Hardness, Bronze*

1. INTRODUCTION

Copper and its alloys exhibit useful properties such as high corrosion resistance, high thermal and electrical conductivity, and excellent machinability (Konečná and Fintová, 2012, Li et al., 2018). Such properties are also present in the Cu-8.5%wt Sn alloy, which has a chemical composition similar to that of the UNS C51200 phosphor bronze, a material commonly used in the manufacture of machine elements and electrical contacts. This bronze, however, has in its as-cast state a eutectoid mixture of high hardness and great brittleness, which is detrimental to subsequent forming processes since this mixture facilitates the propagation of cracks (Afshari et al., 2016).

Various studies have highlighted the effects of manufacturing processes on the microstructure of engineering materials (Miranda et al., 2017, Miranda et al., 2016, Santos, 2017, Santos et al., 2007). Casting is generally the first process that will extensively influence the microstructure of the material and consequently its properties.

It is usual to see a dendritic microstructure in micrographs of binary casting alloys. The characteristic spacings of this kind of microstructure have correlation with thermal variables of solidification, such as cooling rate and tip growth rate (Bouchard and Kirkaldy, 1997).

One can correlate the mechanical properties or the hardness of an alloy with its morphological structure parameters or with thermal variables of solidification by Hall-Petch type equations (Quaresma et al., 2000, Canté et al., 2010, Nascimento et al., 2017, Santos et al., 2017, Nascimento et al., 2018, Nascimento et. al., 2019) or by power functions (Kaya et al., 2009).

The hardness measured at sites belonging to the columnar zone of a unidirectionally solidified cylindrical casting seems to depend not only on their distance from the cooling base but also on the direction (longitudinal or transverse) of the section, where these sites lie, at least for Al-based alloys (Kaya et al., 2009).

Some studies have already been carried out on Cu-Sn alloys, relating thermal variables with microsegregation (Martorano, 1998), thermal variables and use of inoculants with dendritic structure control (Martorano and Capocchi, 2000a) and different casting techniques with the microstructure (Taşliçukur et al., 2012, Machuta and Nová, 2015). As far as one knows, few studies in the literature correlate thermal variables of solidification with (micro)hardness in Cu-Sn alloys. The present work aims to contribute to the study of the Cu-Sn alloys, investigating the correlations between microstructure, thermal solidification variables, and hardness of Cu-8.5wt% Sn alloy in the columnar zone.

2. MATERIALS AND METHODS

The Cu-8.5wt% Sn alloy was prepared with commercially pure tin and UNS C50700 bronze. The heating and melting of the material occurred inside an electrical melting furnace under an argon atmosphere.

The solidification of the molten material occurred inside a unidirectional solidification apparatus. See Fig.1a. The apparatus consists of an adapted furnace with a cooling system, a bipartite mold and some other devices. The bipartite stainless steel mold (7), into which the liquid metal is poured, stands on a steel plate (SAE 1020) (2), which is cooled by a flow of water (1) driven at the beginning of the solidification process. The mold is set inside a furnace provided with electric heaters (9) which can keep the temperature constant by means of a programmable logic controller (8). When the cooling water flow is activated the furnace is immediately switched off. The monitoring of temperatures in the solidification process is carried out by eight thermocouples (3) fixed to the side of the mold. The thermocouples are connected to a data acquisition system (4, 5), allowing visualization and storage of temperature data in a computer (5).

A layer of refractory cement covered the inner surface of the mold (≈ 1.0 mm) and the upper surface of the steel plate (≈ 0.4 mm) too. The thermocouple heights relative to the casting base were 4, 8, 12, 16, 35, 73 and 98 mm. The solidification apparatus was adjusted to reach a temperature of 1150 °C and to keep it until cooling was activated.

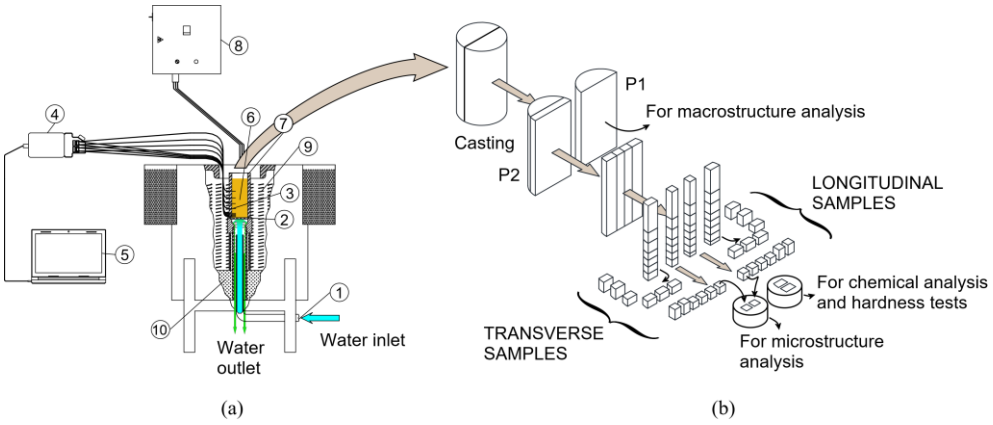

Figure 1. (a) Unidirectional Solidification Apparatus: (1) Water Inlet, (2) Steel base, (3) Thermocouples, (4) Data Acquisition Hardware, (5) Computer and Signal Acquisition Software, (6) Casting, (7) Bipartite Mold, (8) Temperature Controller, (9) Electric Heaters, (10) Insulation Material; (b) Cuts for Preparation of Samples

At approximately 1116 °C the cooling was started and the solidification furnace was switched off . The acquisition of the signals proceeded until the temperature of the furthest thermocouple from the base reached 240 °C. The time and temperature data of each thermocouple were recorded for further analysis.

Figure 1b shows the cuts for preparation of samples. The first longitudinal cut divided the casting into two parts P1 and P2. The flat face of P1 was ground, polished and etched with an acidic ferric chloride solution (52g $FeCl_3$, 325 mL HCl, and distilled H_2O q.s. to 1.0 L) to reveal its macrostructure, while the larger part P2 was subjected to other cuts in order to get 24 samples. Twelve transverse and twelve longitudinal samples were embedded in pairs resulting in six bakelite disks for micrograph and six other disks for chemical analysis and hardness testing. We ground and polished all 24 samples, but we also etched those 12 intended for micrograph with an appropriate ammonium hydroxide solution (40 mL NH_4OH, 40 mL distilled H_2O, 20 mL 3% H_2O_2).

We performed the Vickers hardness testing with 10 kgf (HV10) test load. The mean value of HV10 was calculated by selecting five and three different points of the same sample, respectively. We have determined the chemical composition of the transverse samples by Optical Emission Spectroscopy.

We measured the primary dendrite arm spacing on the micrographs taken from the transverse samples. An inverted platinum microscope and its software for digital image processing and analysis allowed making the necessary micrographs. We determined the average primary dendrite arm spacing on each sample by the triangle method (Gündüz and Çardili, 2002). We drew fifty straight segments per micrograph for that purpose.

We measured the secondary dendrite arm spacing by the linear intercept method (Araujo et al., 2011). We digitally have drawn fifteen straight segments on each micrograph of the longitudinal samples with the aid of Image J software. An average of fifteen values served as the expected value of the secondary dendrite arm spacing of that section.

The Manual Point Count Method allowed determining the volume fraction of the eutectoid mixture in each transverse sample (ASTM, 2011). The method required sixty micrographs (fields) with 1000 × magnification and a mesh of 432 points per micrograph. The use of the Image J software allowed generating this mesh of points on each field. We determined the volume fraction of the eutectoid mixture in each micrograph. The mean of these sixty values yielded the average volume fraction of each transverse sample.

3. RESULTS AND DISCUSSION

The solidification produced a cylindrical casting about 115 mm high after deburring and cleaning. The macrostructure of this casting presented a columnar zone of about 80 mm in length. The analysis of the chemical composition of the transverse samples (at 10, 20, 30, 55 and 70 mm from the base) showed that there was no significant macrosegregation of tin along the height of the casting. The average mass fraction of tin was (8.56 ± 0.05) %Sn.

The software Origin® generated the graphs and the fitting functions of all data sets by the method of least squares.

3.1 Thermal Variables of Solidification

The tip cooling rate was numerically calculated using two consecutive instants recorded by the data acquisition system: one immediately before the local temperature reached the *liquidus* temperature (1026 °C) of the alloy and the other one second later, since the data acquisition was done at a frequency of 1 Hz. The fitting function that correlates the cooling rate ($\dot{T}_L$) of each site with its distance (P) from the cooling base is:

$$\dot{T}_L = (0.0088P + 0.27)^{-2}, \tag{1}$$

where $\dot{T}_L$ is measured in °C/s and P is in mm. The adjusted R^2 (adj. R^2) of Eq.(1) is 0.97.

Let $t_L(P)$ be the time elapsed for the *liquidus* isotherm to reach a particular section expressed as a function of its position. The derivative of $t_L(P)$ with respect to t_L yields the tip growth rate v_L (mm/s) as a function of P:

$$v_L = 66.7(P + 33.9)^{-1}. \tag{2}$$

3.2 Dendrite arm spacings (DAS), position and tip cooling rate

The fitting functions that correlate the primary dendrite arm spacing (λ_1) and the secondary dendrite arm spacing (λ_2) with the position (P) and with the tip cooling rate are:

$$\lambda_1 = 41.5P^{0.43}, \tag{3}$$

$$\lambda_2 = 11.8P^{0.25}, \tag{4}$$

$$\lambda_1 = 273.8\dot{T}_L^{-0.46}, \tag{5}$$

$$\lambda_2 = 35.2\dot{T}_L^{-0.25}, \tag{6}$$

where $[\lambda_1] = [\lambda_2] = \mu m$, $[P]$ = mm and $[\dot{T}_L]$ = °C/s. Both λ_1 and λ_2 are increasing on the interval of P values and decreasing in the respective span of tip cooling rate. The values of adj. R^2 of Eq. (3), (4), (5) and (6) are 0.97, 0.97, 0.89 and 0.91 respectively.

3.3 Volume fraction of eutectoid mixture and tip cooling rate

Figure 2 shows the graph of the volume fraction of eutectoid mixture in transverse samples as a function of the tip cooling rate. The error bars represent a 95% confidence interval.

We can observe that the amount of eutectoid mixture decreases slightly as the tip cooling rate increases.

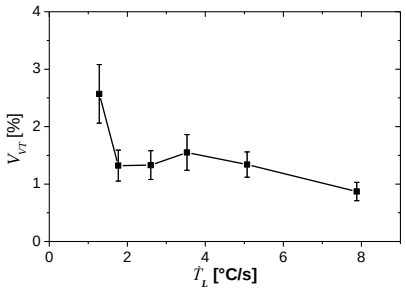

Figure 2. Volume fraction of eutectoid mixture in transverse samples as a function of the tip cooling rate

3.4 Hardness HV10, dendrite arm spacings and thermal variables

Figure 3 shows the data of hardness HV10 plotted against the primary dendrite arm spacing and the secondary dendrite arm spacing.

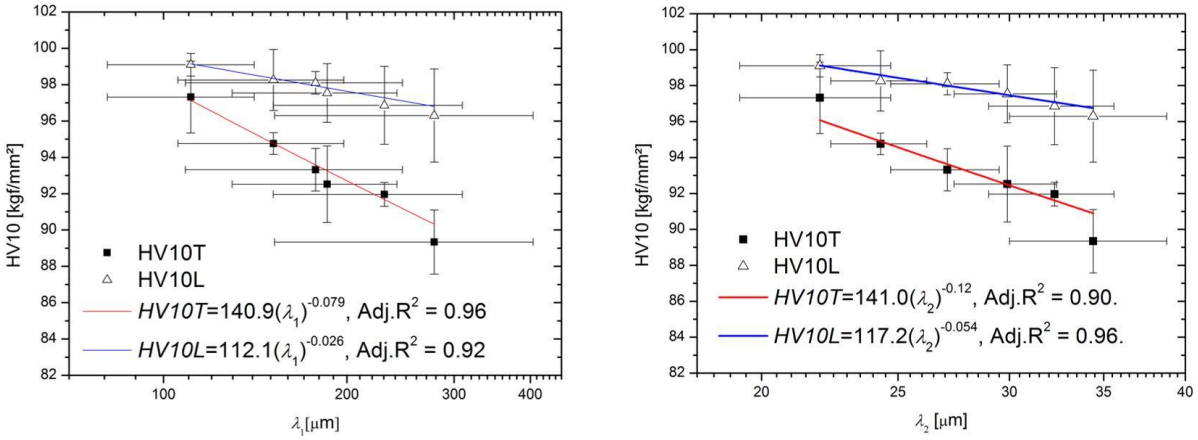

Figure 3. Hardness and DAS: (a) HV10 x λ_1, (b) HV10 x λ_2

Vertical error bars represent the uncertainty in hardness, which is the maximum of two quantities: either the standard deviation or p% of the mean value of hardness on that section (p = 0.5). Horizontal error bars represent one standard deviation of uncertainty in λ_1 and λ_2 measurements.

The fitting curves of hardness decrease slightly on the interval of DAS. The literature reports similar results for some Al-based alloys (Kaya et al., 2009, Aker and Kaya, 2013, Bertelli et al., 2015, Acer et al., 2016).

Figure 4a and 4b show the data of HV10 plotted against the tip growth rate. The error bars represent the same as the vertical error bars of Figure 3.

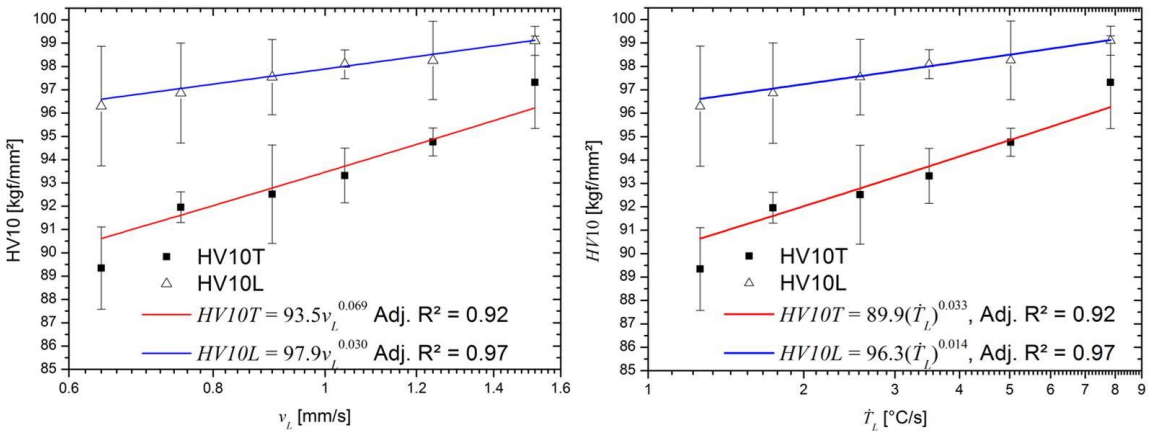

Figure 4. Hardness and thermal variables: (a) HV10 x v_L, (b) HV10 x $\dot{T}_L$

The hardness in both transverse and longitudinal samples tends to increase with tip growth rate. Higher tip growth rates are associated with smaller dendrite spacings. The smaller the dendrite spacings the greater the possibility of piling-up of dislocations, which tends to increase the hardness values of the material. Figure 4c and 4d show the experimental data of hardness plotted against the tip cooling rate, as well as the best fitting curves. The behavior of the hardness *versus* tip cooling rate graph is similar to that of the hardness *versus* tip growth rate graph.

3.5 Hardness fitting function

Hardness can be correlated with morphological structure parameters or with thermal variables of solidification by power functions of the type $HV = aw^b$, where w is a variable and a and b are constants. The values of (a, b) are displayed in Tab. 1. For example: (93.5, 0.069) → $HV10T = 93.5\ (v_L)^{0.069}$.

Table 1. Values of constants *a* and *b* in ordered pair format (*a*, *b*) for each power function of the type $HV = aw^b$

Variable w	$HV10T$ [kgf/mm²]	$HV10L$ [kgf/mm²]
v_L [mm/s]	(93.5, 0.069)	(97.9, 0.030)
$\dot{T}_L$ [°C/s]	(89.9, 0.033)	(96.3, 0.014)
λ_1 [µm]	(140.9, -0.079)	(112.1, -0.026)
λ_2 [µm]	(141.0, -0.12)	(117.2, -0.054)

3.6 Micrographs

Micrographs of some longitudinal and transverse samples are shown in figure 5. Prevalent thermal variables during solidification, DAS and the position of the samples are displayed on the figure. Thermal variables and DAS were calculated by equations (1), (2), (3) and (4).

Figures 5a, 5c and 5e show X-shaped structures that turn up when the primary arms are not exactly parallel to the metallographic section plane and when primary plates are present. Figures 5b, 5d and 5f suggest that there is coalescence of tertiary arms throughout the columnar zone. Figure 5 also indicates that the structures are more refined for positions closer to the cooling base, where the cooling rate and the tip growth rate are higher.

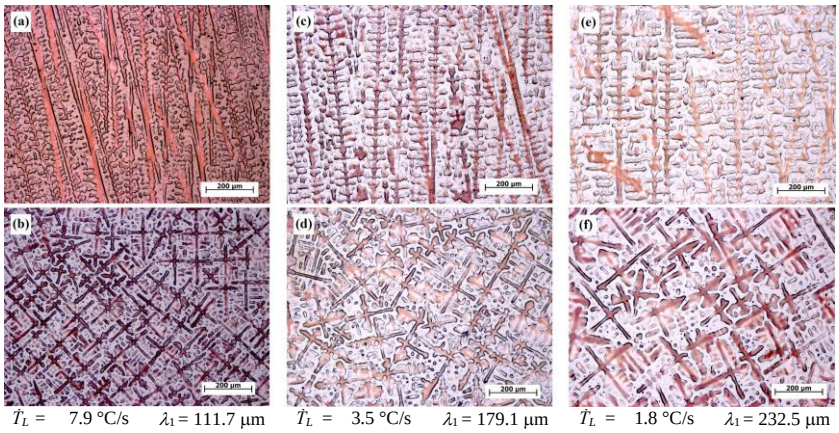

Figure 5. Microstructure of longitudinal (a, c and e) and transverse (b, d and f) sections of the casting

4. CONCLUSIONS

After the analysis of the results, it was possible to conclude the following:

1) Dendrite arm spacings correlate with the tip cooling rate by decreasing power functions: Equations (5) and (6).
2) The hardness in the transverse direction presents changes more accentuated than in the longitudinal one. That implies *b* assumes higher absolute values in the first case, as Tab.1 displays.
3) The volume fraction of eutectoid mixture (a high hardness material) decreases slightly as the tip cooling rate increases.

5. ACKNOWLEGMENTS

The authors thank the research and development staff of Termomecanica São Paulo S.A. for the donation of the research material and the provision of their laboratories for chemical analysis and hardness testing. The authors also thank the Federal Institute of Education, Science and Technology of São Paulo for the provision of its foundry and solidification, metallography and microscopy laboratories and of its machine shops. Finally, the authors thank for the financial support provided by The Brazilian National Council for Scientific and Technological Development (CNPq) and Coordination for the Improvement of Higher Education Personnel (CAPES).

6. REFERENCES

Acer, E., Çadirli, E., Erol, H. and Gündüz, M., 2016. "Effect of Growth rate on the Microstructure and Microhardness in a Directionally Solidified Al-Zn-Mg Alloy", *Metallurgical and Materials Transactions,* Vol. 47A, pp. 3040-3051.

Afshari, E., Ghambari, M. and Farhangi, H., 2016. "Effect of microstructure on the breakage of tin bronze machining chips during pulverization via jet milling", *International Journal of Minerals, Metallurgy and Materials,* Vol. 23(11), pp. 1323-1332.

Aker, A. and Kaya, H., 2013. "Measurements of Microstructural, Mechanical, Electrical, and Thermal Properties of an Al-Ni Alloy", *International Journal of Thermophysics,* Vol. 34, pp. 267-281.

Araujo, I. J. C., da Silva, B. L., Spinelli, J. E. and Garcia, A. (2011) "Evolution of Eutectic Spacing During Unidirectional Solidification of Al-Ni Alloys", *Materials Research-Ibero-American Journal of Materials*, Vol.14(2), pp. 268-273.

ASTM, 2011. *E562-11: Standard Test Method for Determining Volume Fraction by Systematic Manual Point Count*.

Bertelli, F., Brito, C.C., Ferreira, I.L., Reinhart, G., Nguyen-Thi, H., Mangelinck-Nöel, N., Cheung, n. and Garcia, A., 2015. "Colling Thermal Parameters, Microstructure, Segregation and Hardness in Directionally Solidified Al–Sn-(Si;Cu) alloys", *Materials and Design*, Vol. 72, pp. 31-42.

Bouchard, D. and Kirkaldy, J. S., 1997. "Prediction of Dendrite Arm Spacings in Unsteady and Steady-State Heat Flow of Unidirectionally Solidified Binary Alloys", *Metallurgical and Materials Transactions B,* Vol. 28B, pp. 651-663.

Canté, M.V., Spinelli, J.E., Cheung, N. and Garcia, A., 2010. "The Correlation Between Dendritic Microstructure and Mechanical Properties of Directionally Solidified Hypoeutectic Al-Ni Alloys", *Metals and Materials International,* Vol. 16(1), pp. 39-49.

Gündüz, M. and Çardili, E., 2002. "Directional solidification of aluminium–copper alloys", *Materials Science and Engineering A,* Vol. 327, pp. 167–185.

Kaya, H., Gündüz, M., Çadırlı, E. and Maraslı, N., 2009. "Dependency of microindentation hardness on solidification processing parameters and cellular spacing in the directionally solidified Al based alloys", *Journal of Alloys and Compounds,* Vol. 478, pp. 281–286.

Konečná, R. and Fintová, S., 2012. "Copper and copper alloys: casting, classification and characteristic microstructures", in Collini, L. (ed.) *Copper Alloys – Early Applications and Current Performance – Enhancing Processes*. Rijeka, Croatia: Intech, pp. 3-30.

Li, Y., Zhou, R., Li, L., Xiao, H. and Jiang, Y., 2018. "Microstructure and Properties of Semi-solid ZCuSn10P1 Alloy Processed with an Enclosed Cooling Slope Channel", *Metals,* Vol. 8(275), pp. 1-11.

Machuta, J. and Nová, I., 2015. "Monitoring of copper alloys structures during solidification and cooling of castings", *Metal*.

Martorano, M.d.A., 1998. *Efeitos de algumas variáveis de processo na microssegregação da liga Cu-8%Sn* [Tese de Doutorado], São Paulo, Brazil.

Martorano, M.d.A. and Capocchi, J. D. T., 2000a. "Dendrite structure control in directionally solidified bronze castings (Cu-8%Sn)", *International Journal of Cast Metals Research,* (13), pp. 49-57.

Miranda, F., Rodrigues, D., Nakamoto, F.Y., Frajuca, C. and Santos, G.A., 2017. "The Influence of the Sintering Temperature on the Grain Growth of Tungsten Carbide in the Composite WC-8Ni", *Materials Science Forum,* 899, pp. 424-430.

Miranda, F., Rodrigues, D., Nakamoto, F.Y., Frajuca, C., Santos, G.A.d. and Couto, A.A., 2016. "Microstructural Evolution of Composite 8 WC-(Co, Ni): Effect of the Addition of SiC", *Defect and Diffusion Forum,* Vol. 371, pp. 78-85.

Nascimento, M.S., Frajuca, C., Nakamoto, F.Y., Santos, G.A.d. and Couto, A.A., 2017. "Correlação entre variáveis térmicas de solidificação, microestrutura e resistência mecânica da liga Al-10%Si-2%Cu", *Revista Matéria,* Vol. 22(1).

Nascimento, M.S., Franco, A.T.R., Frajuca, C., Nakamoto, F.Y., Santos, G.A.d., and Couto, A.A., 2018. "An Experimental Study of the Solidification Thermal Parameters Influence upon Microstructure and Mechanical Properties of Al-Si-Cu Alloys", *Materials Research*, Vol. 21(5), e20170864. Epub June 18, 2018. https://dx.doi.org/10.1590/1980-5373-mr-2017-0864.

Nascimento, M.S.; Santos, G.A.; Teram, R.; Santos, V.T.; Silva, M.R.; Couto, A.A. "Effects of Thermal Variables of Solidification on the Microstructure, Hardness, and Microhardness of Cu-Al-Ni-Fe Alloys". *Materials* 2019, vol. *12*, pp. 1267.

Quaresma, J.M.V., Santos, C.A. and Garcia, A., 2000. "Correlation between unsteady-state solidification conditions, dendrite spacings, and mechanical properties of Al-Cu alloy"', *Metallurgical and Materials Transactions a-Physical Metallurgy and Materials Science*, Vol. 31(12), pp. 3167-3178.

Santos, G.A., Goulart, P.R., Couto, A.A. and Garcia, A., 2017a. "Primary Dendrite Arm Spacing Effects upon Mechanical Properties of an Al-3w%Cu-1w%Li Alloy", *Properties and Characterization of Modern Materials. Advanced structured materials*: Springer.

Santos, G.A., Neto, C.M., Osório, W.R. and Garcia, A., 2007. "Design of mechanical properties of a Zn27Al alloy based on microstructure dendritic array spacing", *Materials and Design*, Vol. 28(9), pp. 2425-2430.

Santos, G.A.d., 2017. "The importance of metallic materials as biomaterials", *Adv. Tissue Eng. Regen. Med. Open Access*, Vol. 3(1), pp. 300-302.

Taşliçukur, Z., Altuğ, G.S., Polat, Ş., Atapek, Ş.H. and Türedi, E., 2012. "A Microstructural Study on CuSn10 Bronze produced by sand and Investment Casting Techniques", *Metal*.

7. RESPONSIBILITY NOTICE

The authors are the only responsible for the printed material included in this paper.